An Analytical Prediction Model of Balanced and Unbalanced Faults in Doubly-Fed Induction Machines

Frederic Maurer, Trond Leiv Toftevaag, *Membership*, and Jonas Kristiansen Nøland, *Membership*

Post Conference Paper Ref. [23]

Abstract—This paper presents the exact transient solution to the unbalanced and balanced faults in the doubly-fed induction machine (DFIM). Stator currents, rotor currents, and stator fluxes have been validated using simulation and experiment. The work is meant to strengthen and fasten the predictability of large DFIMs in the design stage to comply with mechanical constraints or grid fault issues. Moreover, the analytical approach reduces the computational costs of large-scale stability studies and is especially suited to the initial phase, where a of plethora design computations must be carried out for the DFIM before it is checked for its transient interaction with the power system. The possibility to dynamically estimate the DFIM performance is simplified by original equations derived from first principles. First, case studies of two large $265\,\mathrm{MVA}$ DFIMs are used to verify the analytical approach, and to justify the proposed "large machine approximation" using simulation with an exact match. Finally, laboratory measurements were conducted on a $10.96\,\mathrm{kVA}$ and a $1.94\,\mathrm{kVA}$ DFIM to validate the transient current peaks predicted in the proposed analytic expressions for two-phase and three-phase faults, respectively.

Index Terms—Transient analytical modeling, doubly-fed induction machines (DFIMs), unbalanced short-circuits.

I. Introduction

THE doubly-fed induction machine (DFIM) is a topology that is widely applied in a variety of power generation facilities, such as hydropower [1]–[5] and wind power [6]–[8] applications. In large facilities, there are concerns related to the mechanical design, the control design, as well as to the interaction with the power system [9], where transients can propagate. Constraining the armature currents and torque transients are critical machine-related issues, as their peak values influence the mechanical and grid connection designs. The DFIM must withstand these stresses without any damages, e.g., mechanical vibrations in the winding overhang of large DFIMs.
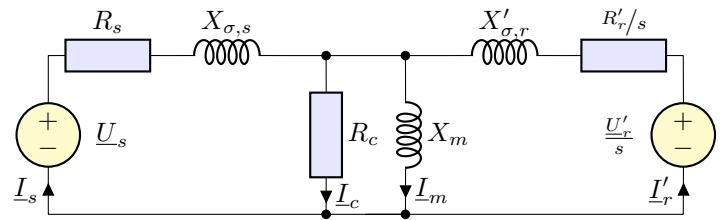
Fig. 1. Equivalent schematic diagram of the DFIM studied herein.

The rotor slip can vary from -10 % to 10% (e.g., in hydropower), or as much as from -30% to 30% (e.g., in wind power). It is, therefore, likely that the DFIM will experience vibration, even during normal operation. For instance, rotor harmonics [10] or even supply induced harmonics [11] can lead to vibrations. Therefore, a user-friendly and simplified analytical approach is needed to give a go/no-go decision for large DFIMs in the design stage. In fact, a detailed numerical model would require huge computational efforts, e.g., finite element (FE) magnetic and mechanical calculation. The main contribution of this paper is formulating an exact analytical method to significantly reduce the computations needed to estimate peak transient torque and currents occurring in DFIMs, where FE is merely used to extract parameters prior to machine construction.

From the grid perspective, the phenomena occurring during a fault-ride through (FRT) event are much more relevant [12]–[15]. In these cases, the grid owner normally requires that the machine can stay connected to the grid after several transient events that might occur. However, the amplitudes of these phenomena are generally lower than for a terminal short-circuit fault (balanced or unbalanced). They do not impact the mechanical design of the generator as the more severe, local ones. Grid faults are usually simulated in generalized numerical simulation environments, such as SIMSEN, as the system topology might be different for every project.

Earlier works on DFIMs have been limited to transient equations for the three-phase short-circuit while ignoring the unbalanced case [16]. Moreover, the three-phase analytical equations that have been derived do not match precisely with

TABLE I
DFIM'S RATED DATA - M1, M2, M3 & M4

Quantity	M1	M2	M3	M4
nom. power (S)	265.5 MVA	265 MVA	10.96 kVA	1.94 kVA
stator volt. (U_s)	18 kV	15.75 kV	230 V	400 V
stator cur. (I_s)	8.5 kA	9.8 kA	27.5 A	2.8 A
mech. speed (n)	158.51 rpm	333.34 rpm	1430 rpm	1420 rpm
stator freq. (f_s)	50 Hz	50 Hz	50 Hz	50 Hz

TABLE II
SIMULATED DFIM - CALCULATED PARAMETERS - MACHINE M1 & M2

Symb.	Quantity	M1	M2
R_s	stator resistance	4.5056 mΩ	3.8183 mΩ
		(≈ 0.0037 pu)	(≈ 0.0041 pu)
R'_r	rotor resistance	1.9364 mΩ	1.5809 mΩ
		(≈ 0.0016 pu)	(≈ 0.0017 pu)
X_s	stator react. (sat.)	2.0912 Ω	2.33731 Ω
		(≈ 1.7136 pu)	(≈ 2.4969 pu)
X_m	magn. react. (sat.)	1.9387 Ω	2.2306 Ω
		(≈ 1.5887 pu)	(≈ 2.3829 pu)
$X_{\sigma,s}$	stator leak. react.	0.1525 Ω	0.1068 Ω
		(≈ 0.1250 pu)	(≈ 0.1140 pu)
$X'_{\sigma,r}$	rotor leak. react.	0.1957 Ω	0.1692 Ω
		(≈ 0.1604 pu)	(≈ 0.1808 pu)

TABLE III
EXPERIMENTAL DFIMS - MEASURED PARAMETERS - M3 & M4

Symbol	Quantity	M3	M4
R_s	cold stator resistance	144.92 mΩ	8.40 Ω
R'_r	cold rotor resistance	231.4 mΩ	10.65 Ω
R_c	core loss resistance	125.88 Ω	842.86 Ω
X_s	stator reactance (sat.)	7.48 Ω	133.39 Ω
X_m	magnetizing reactance (sat.)	7.22 Ω	117.32 Ω
$X_{\sigma,s}$	stator leakage reactance	262.53 mΩ	16.07 Ω
$X'_{\sigma,r}$	rotor leakage reactance	262.53 mΩ	16.07 Ω

the presented test results [16], while this paper proposes not only an exact match with simulation results but also a sufficient match between analytical expression and measurements as well. In [17], the analytical developments are declared as approximate, while the experiment and simulation show only the agreement without explicit comparison, i.e., without placing them on the same figure allowing the reader to judge the fidelity of the approximated expressions developed, whereas our paper does. Recently, other simplified models have been proposed for the DFIM under steady-state and transient operations [18], [19], without considering the short-circuit case. Reference [20] presented a harmonics analysis of the double-output induction generator that also overlooked the short-circuit impact. Other applications of transient models include DFIM controller improvements [21], as well as reducing the computational burden of transient stability studies [22].

This paper takes the transient domain a step further, with an earlier preliminary work already taken as a basis [23]. A complete set of dynamic equations for the induction machine was presented in [24], whereas the well-known expressions for an induction machine were already provided in [25]. However, both of these did not consider the specific case of DFIMs under terminal short-circuits. The original contribution of this study lies in the transient equations for DFIM that are applicable for the "large machine approximation" (refer to [25] for its definition), which are further derived based on the work presented by [24], and specifically adapted for a DFIM. In addition, the exact equations for predicting the unbalanced two-phase fault are also included in this paper, which is in itself a distinguishable contribution relative to the latest literature. The analytic expressions also provide frequency harmonic information, which can be effectively used to ensure that a severe transient might trigger no mechanical eigenmodes over the complete operating range of a large DFIM. Compared to [23], this paper added an experimental validation of the expression developed in the conference paper, provided a complete derivation of the equation set, and extended the range of use to smaller power machines (2 kVA and 11 kVA).

As a first step in this research, the work focuses merely on the machine side and the validation of the transient expressions for a large DFIM. Further studies should integrate grid and converter interactions as well. Analytical expressions have significant time and integration advantages compared to numerical simulation, especially in the design process of large DFIMs, which normally requires between 50-100 iterations (e.g., that number can easily reach up to 1000 simulations

considering several operation points). Therefore, saving time in the transient analysis is highly appreciated.

Several handpicked three-phase, star-connected DFIMs (insulation class F), i.e., M1, M2, M3, and M4, are studied in this paper. Two large 265 MVA-sized machines have been chosen for the theoretical study, which is the highest-rated DFIMs in construction. In addition to M1, M2 was chosen for the additional simulation with a current-controlled rotor converter that had regulator parameters available. M3 and M4 are low-rated machines available in the laboratory. Tables I and II give the rated data and equivalent parameters of M1 and M2 used in the theoretical analysis, made in comparison with SIMSEN. In addition, Tables I and III provide the rated data and estimated parameter values (from measurements)[1] of M3 and M4 used in experimental verification. Fig. 2 present the measured open-circuit characteristic of M3 and M4 with an open rotor. It shows how the stator reactance (X_s) depend on voltage level, where unsaturated values are larger than those in Table III.

The remainder of the paper is organized as follows. Section

---

[1]The leakage reactance is obtained using the classical approach presented in the norm IEEE 112, which permits obtaining the sum of both reactances. Then according to this norm, the results can be divided by two to obtain each reactance, i.e., that is why both are equal. As the DFIM under study is the wound-rotor type, this approach is reasonable and leads to "acceptable results" as both slots should be more or less the same. Another option would have been to compute them using classical analytical computation â but as we did not find any drawing or electrical computation, this path is not practicable.
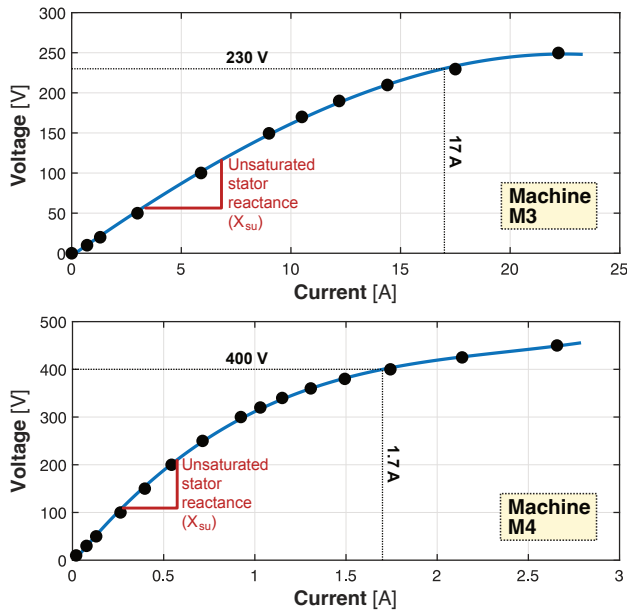
Fig. 2. Standstill open-circuit characteristics of the experimental machines M3 ($10.96\,\text{kVA}$) and M4 ($1.94\,\text{kVA}$) with open rotor circuit. Line-to-line stator voltage plotted against stator current.

II presents the modeling hypothesis and its assumptions before the transient analytical expressions of the DFIM are derived in Section III. Then, in Section IV, validates the constant rotor voltage hypothesis by comparing simulation results with rotor-controlled current and the analytical expressions. Section V validates the torque-estimating equations numerically. Finally, Section VI validates the analytically predicted transient current peaks before Section VII concludes the paper. Appendix A and B provide additional details to the analytical development.

II. THEORETICAL FRAMEWORK AND ASSUMPTIONS

There are some important assumptions taken on board in our work, which are common for transient analysis of large AC machines [25], [26]. The resistance values are taken as constants for a given operating temperature [25]. Moreover, the saturation of the main inductance that may exist prior to the faulty condition is considered by re-adjusting the main inductance to the voltage level prior to the transient event [25]–[27]. These quantities are governed by the saturation of the stator and rotor leakage reactance, where one method postulates to artificially reduce the leakage reactances by 10-20 %, depending on the initial saturation level of the machine [26], to account for this phenomenon. In general, the DFIM can be considered in steady-state with constant torque just before the short-circuit event occurs and as having constant speed during the short-circuit (i.e., ideally high inertia). This hypothesis basically holds for any large DFIM due to its rotor construction leading to an inertia constant >5 s in all cases.

The voltage-sourced inverter (VSI) is modeled with a constant voltage source so that its influence is neglected during the short-circuit [25], that hypothesis will be checked in Section IV. In order to stick with the main focus of the work, no further grid influence is considered at this stage. The VSI is assumed to continue to provide the same rotor voltage as

before the transient, even though the semi-conductors cannot always deliver this. However, in our down-scaled experiments for M3 and M4, the assumption holds. In large-scale reality, there is a resistive crowbar going into operation when the machine and/or the VSI protection decides to fire it [27]. This firing is done to limit the current in the VSI. It takes about 5-10 ms to fire the crowbar, implying that the first and most important current and torque peak will happen without the impact of the crowbar. In the case of the firing of the crowbar, the rotor voltage drops down to zero and is replaced by the resistive crowbar. In order to model the described case, the rotor resistance can be adapted to reflect the crowbar resistance, and the firing of the crowbar is modeled by a rotor voltage step towards zero [27]. However, the detailed action of the crowbar is beyond the scope of this work, but all equations have been derived in a way that it will be very easy to perform that last step on top of our analysis.

The equivalent diagram of the DFIM presented in [25] is recalled in Fig. 1. It follows by Kirchoffs curren law (KCL) in complex variables that

$$\underline{I}_m = \underline{I}_s - \underline{I}_c + \underline{I}'_r. \qquad (1)$$

The mathematical development is performed in the rotating dq-frame to allow exact analytical treatment, while symmetrical component only allow approximated analytical treatment. Moreover, one can easily deduce the voltage equations from Kirchoff's voltage law (KVL), yielding

$$\underline{U}_s = R_s\underline{I}_s + \mathbf{j}(X_{\sigma,s} + X_h)\underline{I}_s + X_h\underline{I}'_r \qquad (2)$$

$$\frac{\underline{U}'_r}{s} = \frac{R'_r}{s}\underline{I}'_r + \mathbf{j}(X'_{\sigma,r} + X_h)\underline{I}'_r + X_h\underline{I}_s, \qquad (3)$$

which have already been established in [25]. Eqs. (2) and (3) are formulated in transient mode, replacing their Laplace-form with time derivative, written in per-unit and omitting the underline (representing the space vector) as

$$u_s = R_s i_s + \left(\frac{d}{dt} + \mathbf{j}\omega_s\right)\psi_s, \qquad (4)$$

$$u_r = R_r i_r + \left(\frac{d}{dt} + \mathbf{j}\Delta\omega\right)\psi_r, \qquad (5)$$

where the $'$-sign is omitted not to create confusion for the transient equation (L'_s and L'_r) of the inductances. The slip (s) incorporated into the definition of $\Delta\omega = s\omega_s$, yielding

$$\Delta\omega = \omega_s - \omega_{\text{mech}} = \omega_s - \omega_s(1 - s) = s\omega_s. \qquad (6)$$

The fluxes in eqs. (4) and (5), with stator subscript 's' and rotor subscript 'r', are given by

$$\psi_s = L_s i_s + L_m i_r, \qquad (7)$$

$$\psi_r = L_m i_s + L_r i_r, \qquad (8)$$

where $L_s = L_{\sigma s} + L_m$ and $L_r = L_{\sigma r} + L_m$.

III. FUNDAMENTAL DFIM TRANSIENT EQUATIONS

This section takes the basics and the assumptions of Section II onboard, and formulates the transient expressions for DFIM analysis. The initial conditions are firste defined before the transient equations for the currents and flux linkages are

derived. Finally, the transient torque expressions provided and the behavior prediction under unbalanced fault conditions are presented.

The derivation of the transient equations has been based on [25], which deviates from the alternative one presented in [24]. In predicting the initial state of the DFIM transients, some initial conditions (written with the subscript 'o') are needed. The stator voltage u_s, the speed n and the mechanical power p_mec are known. From these three parameters, one can deduce the initial values of the stator current (i_s0), rotor (i_r0) current and rotor voltage (u_r0). For the stator and rotor fluxes (used to calculate the torque) their initial conditions are given by

$$u_{so} = R_s i_{s0} + \mathbf{j}\omega_s \psi_{so}, \tag{9}$$

$$u_{ro} = R_r i_{ro} + \mathbf{j}\Delta\omega \psi_{ro}, \tag{10}$$

where eq. (10) is written in the stator reference frame as already stated.

A. Transient Equations for the Stator Currents

Eqs. (4) and (5) are compactly reformatted by setting the derivator d/dt equal to the operator p, yielding

$$u_s = R_s i_s + (p + \mathbf{j}\omega_s)\psi_s \tag{11}$$

$$u_r = R_r i_r + (p + \mathbf{j}\Delta\omega)\psi_r. \tag{12}$$

Then, eq. (8), can be inserted into eq. (12) then solved to obtain the rotor current (i_r) as follows

$$i_\text{r} = \frac{u_\text{r} - (p + j\Delta\omega)L_m i_\text{s}}{R_r\left(1 + (p + j\Delta\omega)T_\text{r}\right)}, \tag{13}$$

where $T_r = L_r/R_r$. Eq. (7) can be inserted into eq. (11) and combined with i_r from eq. (13), yielding

$$
\begin{aligned}
u_\text{s} =& \frac{p^2 + p\left(\frac{T_\text{s}+T_r}{T_\text{s}'+T_\text{r}'} + j(\omega_\text{s} + \Delta\omega)\right)}{L_\text{r}\left(1/T_\text{r} + (p + j\Delta\omega)\right)} i_\text{s} \\
&+ \frac{\frac{1}{T_\text{s}\cdot T_\text{r}'}\left(1 + j\Delta\omega T_\text{r} + j\omega_\text{s}T_\text{s}(1 + j\Delta\omega T_\text{r}')\right)}{L_\text{r}\left(1/T_\text{r} + (p + j\Delta\omega)\right)} i_\text{s} \\
&+ \frac{L_m}{L_\text{r}}\frac{(p + j\omega_\text{s})}{1/T_\text{r} + (p + j\Delta\omega)} u_\text{r},
\end{aligned}\tag{14}
$$

where $T_\text{s} = L_\text{s}/R_\text{s}$, $T_\text{s}' = L_\text{s}'/R_\text{s}$ with $L_\text{s}' = L_{\sigma,s} + L_m L_{\sigma,r}/L_\text{r}$ and $T_\text{r}' = L_\text{r}'/R_\text{s}$ with $L_\text{r}' = L_{\sigma,r} + L_m L_{\sigma,s}/L_\text{s}$. The numerator of eq. (14) is a second order polynom and its simplification using the "large machine approximation" is detailed in Section III-D.

Eq. (14) can also be expressed for the stator current, yielding

$$
\begin{aligned}
i_\text{s} =& \frac{L_\text{r}}{L_\text{s}L_\text{r}'}\frac{p + 1/T_\text{r} + j\Delta\omega}{(p + 1/T_\text{s}' + j\omega_\text{s})(p + 1/T_\text{r}' + j\Delta\omega)} u_\text{s} \\
&+ \frac{L_m}{L_\text{r}}\frac{p + j\omega_\text{s}}{(p + 1/T_\text{s}' + j\omega_\text{s})(p + 1/T_\text{r}' + j\Delta\omega)} u_\text{r}.
\end{aligned}\tag{15}
$$

The transient equation of the stator current can be found by applying an inverse Laplace-transform to the equation. In fact, it is not straightforward to find approximate equation for i_s0, i_s1 and i_s2 (cf. Section III-E for the definition of these currents)

as $\Delta\omega$ has a large amplitude variation and that the equations are not linear in terms of $\Delta\omega$ [27]. The prediction of the current calculation can be found using the exact solution to obtain the zeros of the numerator of eq. (14) as well as the coefficients i_s0, i_s1 and i_s2.

B. Transient Equations for the Stator Flux

The flux eqs. (7) and (8) can be expressed in matrix-form. Inverting the matrix will provide equations of the currents in terms of the fluxes. The stator current (i_s) becomes

$$i_\text{s} = \underbrace{\frac{1}{L_\text{s}'}}_{\alpha} \psi_\text{s} - \underbrace{\frac{L_\text{m}}{L_\text{s}'L_\text{r}}}_{-\beta} \psi_\text{r} = \alpha\psi_\text{s} + \beta\psi_\text{r}, \tag{16}$$

and for the rotor current one obtain

$$i_\text{r} = -\underbrace{\frac{L_\text{m}}{L_\text{s}'L_\text{r}}}_{-\gamma} \psi_\text{s} + \underbrace{\frac{1}{L_\text{r}'}}_{\delta} \psi_\text{r} = \gamma\psi_\text{s} + \delta\psi_\text{r}, \tag{17}$$

where $L_\text{s}' = (L_\text{s}L_\text{r} - L_\text{m}^2)/L_\text{r}$, and $L_\text{r}' = (L_\text{s}L_\text{r} - L_\text{m}^2)/L_\text{s}$. Note that $\beta = \gamma$, conveniently they were defined as two separate variables. Applying eq. (17) into the rotor voltage eq. (12), and solving for the rotor flux (ψ_r) leads to

$$\psi_\text{r} = \frac{u_\text{r} - R_\text{r}\gamma\psi_\text{s}}{R_\text{r}\delta + (p + j\Delta\omega)}. \tag{18}$$

The resulting eq. (18) can be incorporated into the stator voltage eq. (11), then solved in terms of ψ_s, yielding

$$\psi_\text{s} = \frac{\left(R_\text{r}\delta + (p + j\Delta\omega)\right)u_\text{s} - R_\text{s}\beta u_\text{r}}{\left(R_\text{s}\alpha + (p + j\omega_\text{s})\right)\left(R_\text{r}\delta + (p + j\Delta\omega)\right) - R_\text{s}R_\text{r}\beta\gamma}, \tag{19}$$

$$
\begin{aligned}
\psi_\text{s} =& \frac{R_\text{r}\delta + (p + j\Delta\omega)}{\left(R_\text{s}\alpha + (p + j\omega_\text{s})\right)\left(R_\text{r}\delta + (p + j\Delta\omega)\right) - R_\text{s}R_\text{r}\beta\gamma} u_\text{s} \\
&- \frac{R_\text{s}\beta}{\left(R_\text{s}\alpha + (p + j\omega_\text{s})\right)\left(R_\text{r}\delta + (p + j\Delta\omega)\right) - R_\text{s}R_\text{r}\beta\gamma} u_\text{r}.
\end{aligned}\tag{20}
$$

C. Transient Equation for the Rotor Current

The stator voltage equation, eq. (11), is solved to obtain i_s, which will be inserted into the rotor current equation, eq. (13), which will be solved to obtain the desired transfer function. The result of these manipulations can then be inserted into the rotor voltage equation, yielding

$$u_\text{r} = R_\text{r}\left(1 + (p + j\Delta\omega)T_\text{r}\right)i_\text{r} + \left(p + j\Delta\omega\right)L_\text{m}i_\text{s}, \tag{21}$$

$$
\begin{aligned}
u_\text{r} =& \frac{R_\text{r}R_\text{s}\left(1 + (p + j\Delta\omega)T_\text{r}\right)\left(1 + (p + j\omega_\text{s})T_\text{s}\right)}{R_\text{s}\left(1 + (p + j\omega_\text{s})T_\text{s}\right)} i_\text{r} \\
&- \frac{(p + j\Delta\omega)(p + j\omega_\text{s})L_\text{m}^2}{R_\text{s}\left(1 + (p + j\omega_\text{s})T_\text{s}\right)} i_\text{r} \\
&+ \frac{(p + j\Delta\omega)L_\text{m}}{R_\text{s}\left(1 + (p + j\omega_\text{s})T_\text{s}\right)} u_\text{s}.
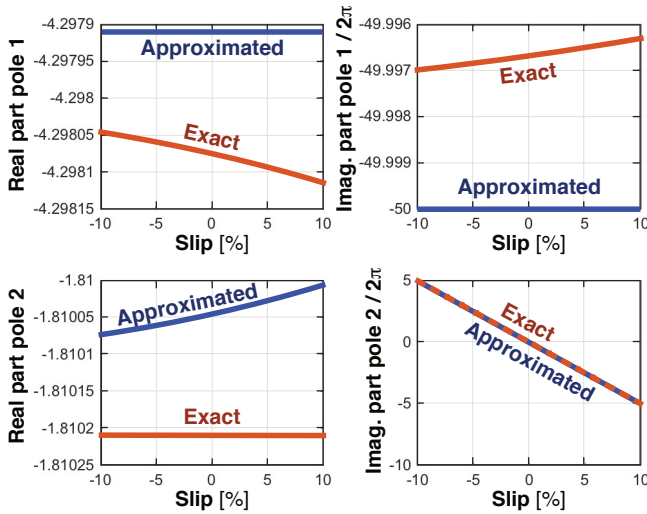\end{aligned}\tag{22}
$$

Fig. 3. Evolution of the poles p_1 and p_2 in function of $\Delta\omega$ for M1. Adapted from preliminary work [23].

Eq. (22) can be formulated in terms of i_r, leading to the rotor current expression. Reference [27] presents a validation using the SIMSEN numerical environment for simulating the presented rotor current equations and got a good agreement between analytical and numerical expressions.

D. Simplification of the Poles of the Transfer Function

Recalling the numerator of eq. (14) leads to

$$p^2 + p[\frac{T_\mathrm{s} + T_\mathrm{r}}{T_\mathrm{s}' + T_\mathrm{r}'} + j(\omega_\mathrm{s} + \Delta\omega)]$$
$$+ \frac{1}{T_\mathrm{s} \cdot T_\mathrm{r}'}[1 + j\Delta\omega T_\mathrm{r} + j\omega_\mathrm{s}T_\mathrm{s}(1 + j\Delta\omega T_\mathrm{r}')] = 0. \quad (23)$$

In the field of large electrical machines, the following inequalities can be considered as fulfilled (refer to [25])

$$T_\mathrm{r} > T_\mathrm{s} \gg T_\mathrm{r}' \gg T_\mathrm{s}' \gg 1/\omega_\mathrm{s}. \quad (24)$$

The inequalities are also called the "large machine approximation". On purpose, $\Delta\omega$ was deliberately not used in the inequalities as it can change in the range $-0.1\omega_\mathrm{s}$ to $0.1\omega_\mathrm{s}$. It simplifies the equation of the poles and shows that the poles (p_1 and p_2) can be expressed as

$$p_1 = -1/T_\mathrm{s}' - j\omega_\mathrm{s}, \quad (25)$$
$$p_2 = -1/T_\mathrm{r}' - j\Delta\omega, \quad (26)$$

at leading order. Further treatment of this part can be found in [23], [27]. Fig. 3 shows the evolution if the real part and imaginary part of p_1 and p_2 for different values of $\Delta\omega$. One can see that at leading order, the poles behave like the simplified equations predicts.

E. Torque Harmonics for a Three-Phase Short-Circuit, or Three-Phase Faulty Synchronization

In order to exclude any excitation of a mechanical eigenmode in the stator or rotor of the generator, one needs to determine the frequency of the torque harmonics. From eq. (15) one can deduce that the stator current is given by

$$i_\mathrm{s} = i_\mathrm{s0} + i_\mathrm{s1} \exp(-t/T_\mathrm{s}') \sin(\omega_\mathrm{s}t)$$
$$+ i_\mathrm{s2} \exp(-t/T_\mathrm{r}') \sin(\Delta\omega t) \quad (27)$$

where i_s0, i_s1 and i_s2 (the detailed expression are given in Sec. VIII-A) are obtained from the corresponding transfer function. Similarly, the stator flux is obtained from the stator current, starting from eq. (20), yielding

$$\psi_\mathrm{s} = \psi_\mathrm{s0} + \psi_\mathrm{s1} \exp(-t/T_\mathrm{s}') \sin(\omega_\mathrm{s}t)$$
$$+ \psi_\mathrm{s2} \exp(-t/T_\mathrm{r}') \sin(\Delta\omega t), \quad (28)$$

where ψ_s0, ψ_s1, ψ_s2 (the detailed expression are given in Sec. VIII-B) are obtained from the corresponding transfer function. Finally, the torque (T_{em}) is given by

$$T_{em} = \frac{3}{2} \cdot p \cdot \mathbb{Im}\{\psi_\mathrm{s}^* \cdot i_\mathrm{s}\}. \quad (29)$$

The interesting part of the torque harmonics is to identify if there could be any resonance between the mechanical system and the foundation, i.e., it is not mandatory to calculate each component. Its frequency dependence leads to

$$f_1 = 2\Delta\omega \quad (30)$$
$$f_2 = \omega_\mathrm{s} \pm \Delta\omega \quad (31)$$
$$f_3 = \omega_\mathrm{s} \quad (32)$$
$$f_4 = 2\omega_\mathrm{s}. \quad (33)$$

F. Modelling the Two-Phase Short-Circuit

In the current research literature, no exact analytical expression for the current or torque of a two-phase short-circuit in the dq-rotating frame have been proposed [28], [29]. Based on a previous works on the DC-Decay tests (i.e., two-phase short-circuit) in a synchronous machine [29], the two-phase short-circuit was characterised by the following equation

$$u_a = u_b. \quad (34)$$

Eq. (34) imply that two voltages will be clamped to each other after the short-circuit. In addition to this, if the machine is supposed to be star-connected, yields as the following relations.

$$u_\mathrm{a} + u_\mathrm{b} + u_\mathrm{c} = 0$$
$$2u_\mathrm{a} + u_\mathrm{c} = 0. \quad (35)$$

In order to obtain the voltages after the short-circuit, the reaction of the voltage on the open phase c must be known or assumed known after the event. Prior to the short-circuit, the phase voltage of c is given neither by the machine (through the induced voltage) or by the grid. Just after the fault (a few milliseconds after), the currents in the machine will not have any discontinuity. The currents and the flux linkages are state variables, so that the voltage in phase c will remain the same. The terminal voltage of phase c, is not affected by the short-circuit, will not change. As a result,

$$u_\mathrm{c} = u_\mathrm{s}, \quad (36)$$

where $u_{\rm s}$ is the stator voltage phasor before the short-circuit. In this case, it is important to keep Park's reference frame aligned with the stator voltage in order to get a real number. From this understanding, the stator voltage in the abc-frame is known before and after the short-circuit, yielding

$$u_{\rm a} = -u_{\rm c}/2, \tag{37}$$

$$u_{\rm b} = -u_{\rm c}/2, \tag{38}$$

$$u_{\rm c} = u_{\rm c}. \tag{39}$$

After some trivial trigonometric operations, one obtains the voltage in the rotating frame, yielding

$$u_d = -\frac{u}{2}\sin(2\omega_{\rm s}t) \tag{40}$$

$$u_q = -\frac{u}{2}(1+\cos(2\omega_{\rm s}t)), \tag{41}$$

which is an original contribution of this work and have also been validated with measurement performed on a large AC machine, as preliminary presented in [27]. In summary, the torque harmonics appearing during a two-phase short-circuit or faulty synchronisation, the technique described in this subsection uses the voltage eqs. (40) and (41).

IV. VERIFICATION OF THE CURRENT EQUATIONS

This section presents the validation of the current equation for two-phase and three-phase stator short-circuits starting from the no-load condition. The analytical equations are compared to the response obtained with a SIMSEN simulation model with current regulation (rotor and stator). M2 was chosen because it is the only machine where regulator parameters were readily available. The current regulation is derived from [30], [31], which provides information regarding the regulation and the derivation of the parameters of the regulators). To keep the simulation model simple, the rotor current regulation has no cross-branch I-regulator, leading to a slightly less rapid current control and some oscillation during the transients. A solution to that problem exists and has been implemented in hydropower plant applications but is not relevant for this paper as they only impact the speed at which the regulator reacts to current transients [31].

Fig. 4 presents the comparable curves obtained for the three-phase and two-phase short-circuits, respectively. The first current peaks are quasi-identical on both, which is expected since the regulator needs some time to respond to the short-circuit and that no active short-circuit current control exists. Then, there is a certain damping due to the presence of the current control that reduces the current with respect to the analytical computation, which has no current control at all.

In conclusion, the simplified modeling assessed in Fig. 4, which assumes that a constant rotor voltage source can replace the full converter model and controls, can be considered validated via simulations. If no active short-circuit current control occurs, the results from the analytical expressions match the curves obtained using a complex simulation model. In the sustained short-circuit mode, some discrepancies will inevitably occur, but they are not the main topic of this paper, respectively, beyond the scope of this paper.
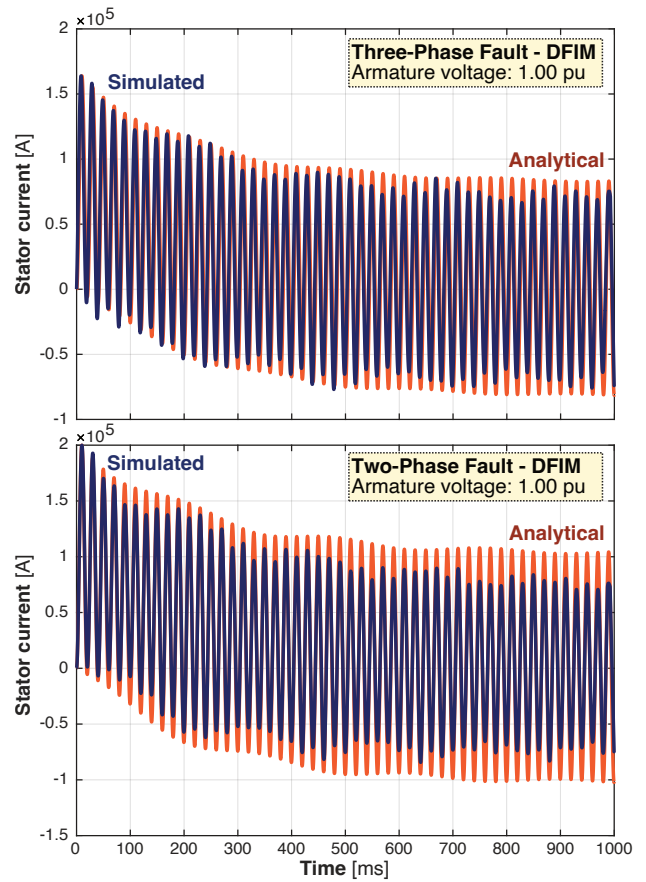

Fig. 4. Stator current (phase a) for a two-phase and three-phase short-circuit from no-load with rated speed and voltage using rotor-current regulated M2.

V. VERIFICATION OF THE TORQUE EQUATIONS

This section presents the validation of the analytical equations developed in Section III for an ASM and DFIM at rated load operation. The verification of the torque is done in the SIMSEN numerical software environment using the parameters defined in Table II (i.e., handpicked simulation case study). SIMSEN assumes an equivalent diagram as given in Fig. 1 and applies the same hypothesis as the one defined in Section II. The electrical machine is connected to the grid on both stator- and rotor-side converters and operated at rated operation before the short-circuit. The analytical equations are compared to numerical solutions. Practically speaking, one enters the same parameters (refer to Table II) and initial conditions and compares the output. The limitations of this confirmation merely depend on the modelling hypothesis that have been proposed. Equivalent parameters for the ASM (i.e., asynchronous machine) and the DFIM (i.e., doubly-fed induction machine) were the same. The ASM is, therefore, a virtual machine, while the DFIM can be considered as the real case. The ASM case was only used to simplify the model and to have a richer validation study. The DFIM is operating at rated conditions (over-excited) before the fault, while the ASM is operating at the same equivalent operating point (same active power) before the short-circuit for both the two-phase and three-phase short-circuit. As the verification for the two-

phase short-circuit only depends on the stator voltage equation, it has been decided to perform it only on the ASM, i.e., the simplest case. Given this premise, the two-phase validation for the DFIM case is implicit. Fig. 5 present the transient air-gap torque curves for the ASM machine in three-phase and two-phase short-circuit, and DFIG in the case of a three-phase short-circuit. Finally, it can be observed that all transient curves agrees well with the simulated curves in SIMSEN.
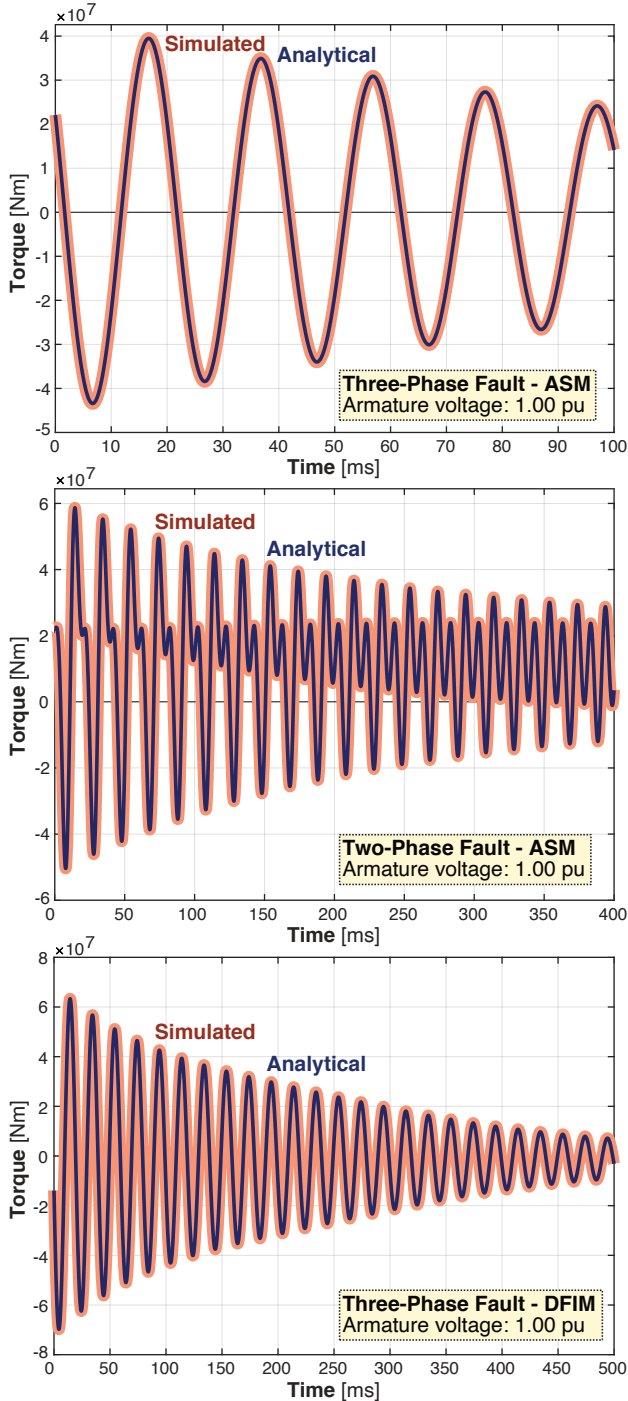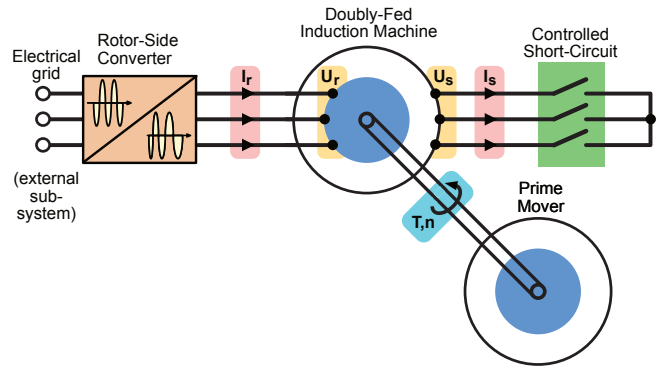

Fig. 6. Schematic description of the experimental test setup (M3 & M4).
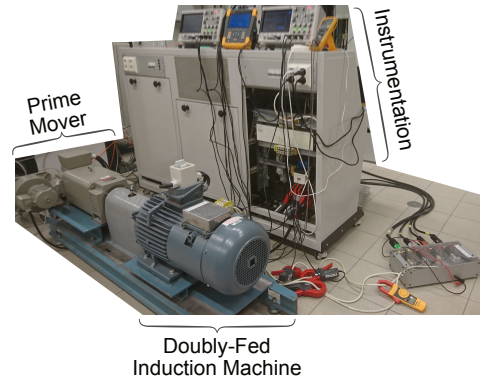

Fig. 7. Picture of experimental test rig (M3).

VI. EXPERIMENTAL VALIDATION OF CURRENT PEAKS

This section extends the verification made in Section IV by providing an experimental validation. The test rig is illustrated and depicted in Figs. 6 and 7. Herein, the rotor-side converter (RSC) has a maximum transient rating of $250\,\text{kVA}$ and $400\,\text{A}$. By intention, the stator voltage have been reduced to avoid entering into the current limitation mode of the RSC so that no coupling of the stator with the grid can be considered. In addition, the main goal of the validation is to measure short-circuits (two-phase and three-phase) from no-load, considering the fact that a load short-circuit has the same expressions [27]. This reduction voltage also limits the transient torques, which is preferred due to the mechanical limitation in the laboratory. There was no additional rotating inertia on the shaft-line, and the rotational speed was only partially maintained by the speed regulator of the prime mover (i.e., the DC-machine). Therefore, some slight speed changes will unavoidably occur and perturbed the measurements.

Prior to the short-circuit, the machine was operated in no-load condition, with the rotor fed by the RSC, with a low stator voltage. The fault is established by closing the short-circuit contactor on the stator side, which induces no redundancy (i.e., confirmed by the contactor closing curves). Then, the stator currents was recorded using a digital storage oscilloscope and plotted against the simulated transient curves. The process was similar for M3 and M4. The short-circuit inception corresponds to a zero-crossing of the voltage of phase a, so with angle of $0°$.
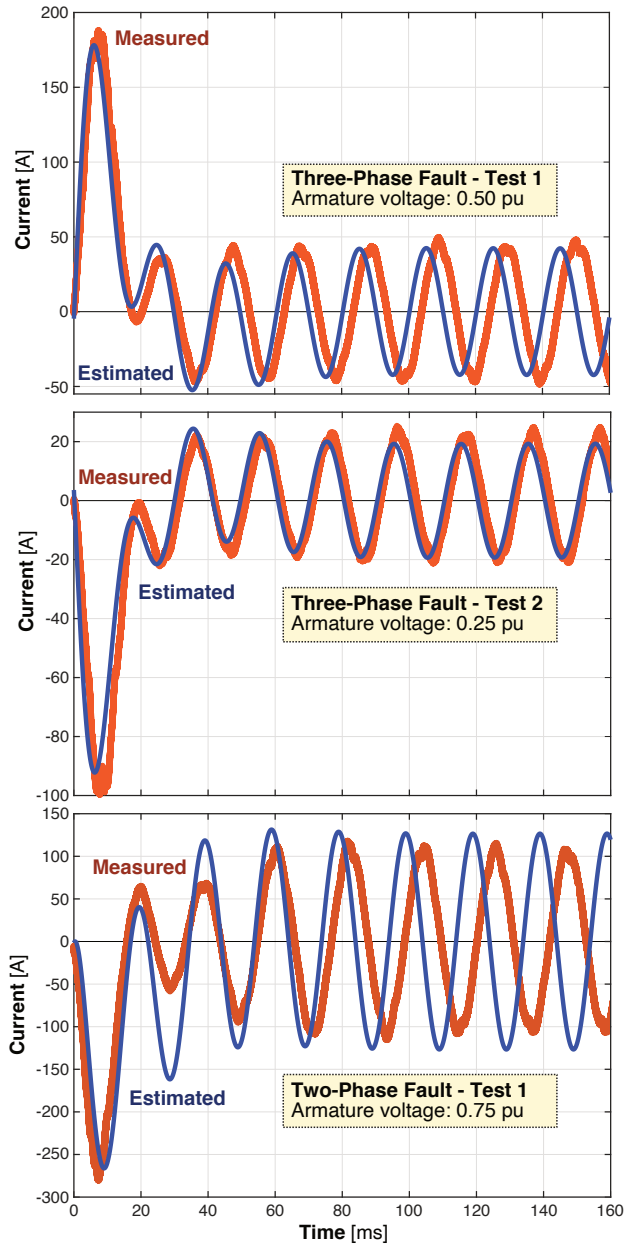

Fig. 5. Transient torque asynchronous with fault event initiated at $0\,\text{ms}$ for M1, with profile given by eq. (29). ASM has short-circuited rotor, while DFIM has constant voltage-fed rotor. Steady constant torque was assumed before the short-circuit. Adapted from preliminary work [23].

Fig. 8. Experimental results of M3 ($10.96\,\mathrm{kVA}$ DFIM) with fault initiated at $0\,\mathrm{ms}$. Estimated curves were solved by eq. (15). Speed was $1350\,\mathrm{rpm}$ ($50\,\mathrm{Hz}$ electrical). The base armature voltage is $230\,\mathrm{V}$.

A. Experimental Results of Machine M3

Fig. 8 presents the three individual tests done on machine M3. Test 1 was done at $50\,\%$ of rated voltage. There is small speed change leading to the observed frequency sweep (due to lack of rotating inertia installed). The frequency sweep is not present for test 2 done at $25\,\%$ armature voltage. The observed current peaks confirm the computation model. For the two-phase fault, the agreement was worst for the first current peak, while a small frequency sweep due to the same above-mentioned phenomenon. However, the steady-state short-circuit current and the first peak are really well estimated, while only the second and third peak deviates from the estimated one (i.e., over-estimated). This phenomena is an
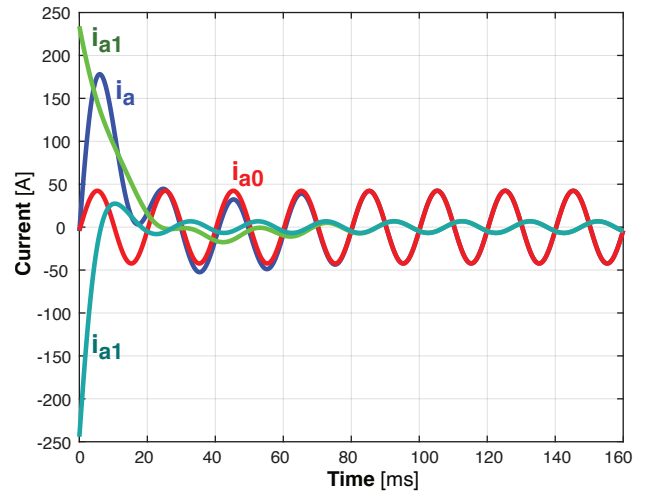

Fig. 9. Detailed computation of each stator current component of the stator three-phase short-circuit current with an armature voltage of $0.5\,\mathrm{pu}$ for M3 ($10.96\,\mathrm{kVA}$ DFIM) with fault initiated at $0\,\mathrm{ms}$. Speed was $1350\,\mathrm{rpm}$ ($50\,\mathrm{Hz}$ electrical). The base armature voltage is $230\,\mathrm{V}$.

issue of further work to determine if this effect is coming of the test platform, considering the simulated M1 agreed well for the whole transient envelope.

Fig. 9 shows the current decomposition for M3 (three-phase short-circuit). After the transient, which is governed by the component 1 and 2, the machine goes into sustained short-circuit operation given by the 0-component. It is interesting to note that the peak is driven by the difference between the components 1 and 2.

B. Experimental Results Machine M4

Fig. 10 presents the 4 tests done on machine M4. Test 1 was done at $100\,\%$ of rated voltage. For this reason, there is a significant transient speed change occurring, leading to the observed frequency sweep (due to lack of rotating inertia). However, the frequency sweep is not present for test 2 done at $50\,\%$ armature voltage and for test 3 done at $25\,\%$ of the nominal voltage. Observed for the two-phase fault, a very good agreement is seen for the first current peak and a small frequency sweep due to the same above-mentioned phenomenon. The steady-state short-circuit current is also well estimated, while only the second and third peak deviates slightly from our estimations. In general, the measurements tend to showcase that the speed change could be the main origin of errors, but other factors could also be involved. The two-phase fault has the highest peaks for same voltage.

Fig. 11 shows the current decomposition for M3 (two-phase short-circuit). After the transient, which is governed by the component 1 and 2, the machine goes into sustained short-circuit operation given by the 0-component and by the 3-component (due to the two-phase pole). It is interesting to note that the peak is driven by the difference between the components 1 and 2.

VII. CONCLUSION

This paper simplifies the transient faulty analysis of double-fed induction machines (DFIMs) by proposing an exact ana-
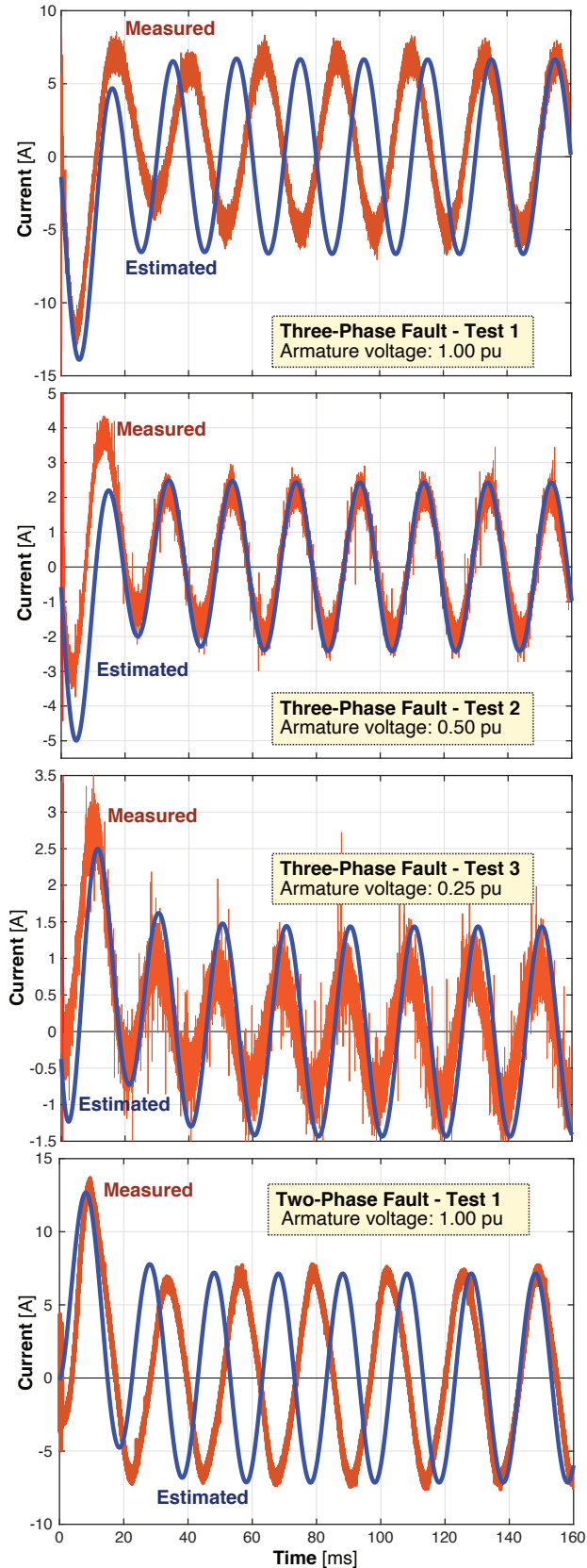
Fig. 10. Experimental results of M4 (1.94 kVA DFIM) with fault initiated at 0 ms. Estimated curves were solved by eq. (15). Speed was 1350 rpm (50 Hz electrical). The base armature voltage is 400 V.
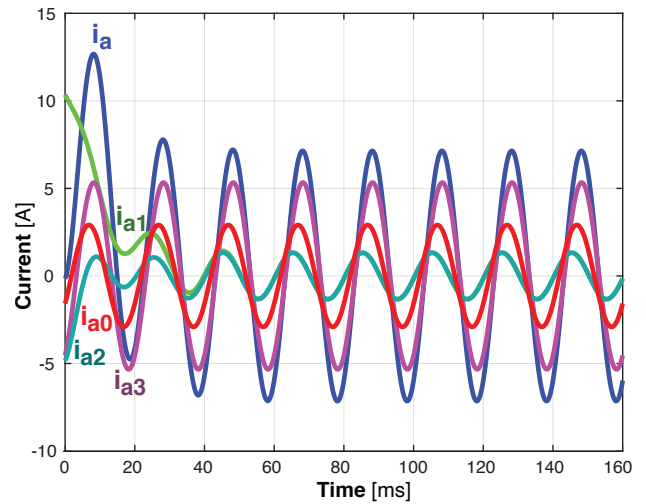

Fig. 11. Detailed computation of each stator current component of the stator three-phase short-circuit current with an armature voltage of 0.5 pu for M4 (1.94 kVA DFIM) with fault initiated at 0 ms. Speed was 1350 rpm (50 Hz electrical). The base armature voltage is 400 V.

lytical model. The framework provides an accurate indication of the harmonic components in the transient and an estimation of the peak torque and currents during faulty events. The approach is in excellent agreement with a detailed numerical model. In addition, the "large machine approximation" is introduced for the analytical model, and it is shown to be valid for the case study of machine M1. Moreover, the constant rotor voltage hypothesis has been validated numerically by a simplified rotor current-controlled simulation model. Finally, two other case studies of experimentally tested machines show that the transient peaks in the armature current amplitudes correspond well with our analytical model, including balanced three-phase faults and unbalanced two-phase short-circuits, respectively. In general, the predictability of our analytic approach can be used to guide the mechanical design of large power conversion facilities, such as variable-speed hydropower and wind power plants. In future research items, complete modeling of the rotor-side converter (RSC) and its control actions can be incorporated in more detail, if needed, for the particular application.

Further work will focus on the integration with the grid, the rotor-side converter (RSC), and especially on the rotor current saturation due to the active current limitation of the RSC.

VIII. APPENDIX

A. Expressions for the Stator Current (i_{s0}, i_{s1} and i_{s2})

A demonstrated in [27], there are no simplified expressions for the stator current as the slip varies between -10% and

+10%. One must therefore compute the exact expression for each speed. To keep the expression readable and simple, the derivation uses matrix-expression. The equations for to obtain the 3phases short-circuit are prenseted in detail hereafter. Due to space limitations, the derivation for the 2phase short-circuit is left over but it follows exactly the same principle. The stator current is given for the 3phase short-circuit by

$$i_s = i_{s0} + i_{s1} \exp(-t/T'_s) \sin(\omega_s t)$$
$$+ i_{s2} \exp(-t/T'_r) \sin(\Delta \omega t) \tag{42}$$

where i_{s0}, i_{s1} and i_{s2} will be determined hereafter. Defining the zero (z_i) of the transfer function (Eq. 15) by

$$z_i = -1/T_r - j\Delta\omega \tag{43}$$

leads to the following expression for i_{s0}

$$i_{s0} = -u_{s0} \frac{z_i}{p_1 * p_2} \frac{T_r}{R_s T_s T'_r} \tag{44}$$

where p_1 and p_2 are the pole of the transfer function (Eq. 15). i_{s1} and i_{s2} are given by

$$i_{s1} = u_{s0}\zeta \frac{T_r}{R_s T_s T'_r} \tag{45}$$

$$i_{s2} = u_{s0}\eta \frac{T_r}{R_s T_s T'_r} \tag{46}$$

where ζ and η can be obtained using a matrix-approach. The matrix approach comes from the separation of variables to be done (leading to 2 equations with 2 unkown) when inverting Eq. 15 to transform it back to the temporal space. The matrix approach leads to a Ax=b equation to be solved. Defining the b-vector as

$$b = \begin{pmatrix} \frac{z_i}{p_1 * p_2} \\ \frac{z_i}{(p_1 * p_2)(p_1 + p_2) - 1} \end{pmatrix} \tag{47}$$

and the A-matrix as

$$A = \begin{pmatrix} 1 & 1 \\ p_2 & p_1 \end{pmatrix} \tag{48}$$

leads to the following expression for ζ and η

$$\begin{pmatrix} \zeta \\ \eta \end{pmatrix} = A^{-1}b. \tag{49}$$

B. Expressions for the Stator Flux (ψ_{s0}, ψ_{s1}, ψ_{s2})

To obtain the detailed expression for the stator flux, one uses the same principle as for the stator current (refer to section VIII-B for the detailed process). The stator flux is given by

$$\psi_s = \psi_{s0} + \psi_{s1} \exp(-t/T'_s) \sin(\omega_s t)$$
$$+ \psi_{s2} \exp(-t/T'_r) \sin(\Delta \omega t), \tag{50}$$

where ψ_{s0}, ψ_{s1}, ψ_{s2} will be computed hereafter.

Defining the zero (z_ψ) of the transfer function (Eq. 20) by

$$z_\psi = -R_r\delta - j\Delta\omega \tag{51}$$

leads to the following expression for ψ_{s0}

$$\psi_{s0} = -u_{s0} \frac{z_\psi}{p_1 * p_2} \tag{52}$$

where p_1 and p_2 are the pole of the transfer function (Eq. 20). ψ_{s1} and ψ_{s2} are given by

$$\psi_{s1} = u_{s0}\zeta_\psi \tag{53}$$
$$\psi_{s2} = u_{s0}\eta_\psi \tag{54}$$

where ζ_ψ and η_ψ can be obtained using a matrix-approach. This approach leads to a Ax=b equation to be solved. Defining the b-vector as

$$b = \begin{pmatrix} \frac{z_\psi}{p_1 * p_2} \\ \frac{z_\psi}{(p_1 * p_2)(p_1 + p_2) - 1} \end{pmatrix} \tag{55}$$

and the A-matrix as

$$A = \begin{pmatrix} 1 & 1 \\ p_2 & p_1 \end{pmatrix} \tag{56}$$

leads to the following expression for ζ and η

$$\begin{pmatrix} \zeta_\psi \\ \eta_\psi \end{pmatrix} = A^{-1}b. \tag{57}$$

C. Expressions for the stator rotor (i_{r0}, i_{r1} and i_{r2})

The rotor current is given for the 3phase short-circuit by

$$i_r = i_{r0} + i_{r1} \exp(-t/T'_s) \sin(\omega_s t)$$
$$+ i_{r2} \exp(-t/T'_r) \sin(\Delta \omega t) \tag{58}$$

where i_{r0}, i_{r1} and i_{r2} will be determined hereafter.

Defining the zero (z_r) of the transfer function (Eq. 22) by

$$z_r = -j\Delta\omega \tag{59}$$

leads to the following expression for i_{r0}

$$i_{r0} = -u_{s0} \frac{z_r}{p_1 * p_2} \frac{x_h}{x_h^2 - x_s x_r} \tag{60}$$

where p_1 and p_2 are the pole of the transfer function (Eq. 22). i_{r1} and i_{r2} are given by

$$i_{r1} = u_{s0}\zeta_r \tag{61}$$
$$i_{r2} = u_{s0}\eta_r \tag{62}$$

where ζ_r and η_r can be obtained using a matrix-approach. This approach leads to a Ax=b equation to be solved. Defining the b-vector as

$$b = \begin{pmatrix} \frac{z_r}{p_1 * p_2} \\ \frac{z_r}{(p_1 * p_2)(p_1 + p_2) - 1} \end{pmatrix} \tag{63}$$

and the A-matrix as

$$A = \begin{pmatrix} 1 & 1 \\ p_2 & p_1 \end{pmatrix} \tag{64}$$

leads to the following expression for ζ and η

$$\begin{pmatrix} \zeta_r \\ \eta_r \end{pmatrix} = A^{-1}b. \tag{65}$$

REFERENCES

[1] A. Joseph, K. Desingu, R. R. Semwal, T. R. Chelliah, and D. Khare, "Dynamic performance of pumping mode of 250 mw variable speed hydro-generating unit subjected to power and control circuit faults," *IEEE Trans on Energy Convers.*, vol. 33, no. 1, pp. 430–441, 2018.

[2] R. Kumari, K. K. Prabhakaran, K. Desingu, T. R. Chelliah, and S. V. A. Sarma, "Improved hydroturbine control and future prospects of variable speed hydropower plant," *IEEE Trans. Ind. Appl.*, vol. 57, no. 1, pp. 941–952, 2021.

[3] K. Desingu, R. Selvaraj, A. K. Birudula, and T. R. Chelliah, "Thermal performance improvement in multi-megawatt power converters serving to asynchronous hydro generators operating around synchronous speed," *IEEE Trans. Energy Convers.*, pp. 1–1, 2020.

[4] A. Joseph, R. Selvaraj, T. R. Chelliah, and S. V. A. Sarma, "Starting and braking of a large variable speed hydrogenerating unit subjected to converter and sensor faults," *IEEE Trans. Ind. Appl.*, vol. 54, no. 4, pp. 3372–3382, 2018.

[5] A. Joseph, T. R. Chelliah, R. Selvaraj, and K.-B. Lee, "Fault diagnosis and fault-tolerant control of megawatt power electronic converter-fed large-rated asynchronous hydrogenerator," *IEEE J. Emerg. Sel. Top. Power Electron.*, vol. 7, no. 4, pp. 2403–2416, 2019.

[6] M. Abdeen, H. Li, S. Kamel, A. Khaled, M. El-Dabah, M. Kharrich, and H. F. Sindi, "A recent analytical approach for analysis of sub-synchronous resonance in doubly-fed induction generator-based wind farm," *IEEE Access*, vol. 9, pp. 68 888–68 897, 2021.

[7] X. Wang, D. Liu, and H. Polinder, "Improving annual energy production of doubly-fed induction generators," *IEEE Trans. Energy Convers.*, pp. 1–1, 2021.

[8] P. Chao, W. Li, X. Liang, S. Xu, and Y. Shuai, "An analytical two-machine equivalent method of dfig-based wind power plants considering complete frt processes," *IEEE Trans. Power Syst.*, pp. 1–1, 2021.

[9] M. Debouza and A. Al-Durra, "Grid ancillary services from doubly fed induction generator-based wind energy conversion system: A review," *IEEE Access*, vol. 7, pp. 7067–7081, 2019.

[10] Yong Liao, Li Ran, G. A. Putrus, and K. S. Smith, "Evaluation of the effects of rotor harmonics in a dfig with harmonic induced speed ripple," *IEEE Trans. Energy Convers.*, vol. 18, no. 4, pp. 508–515, 2003.

[11] S. Djurovic, D. S. Vilchis-Rodriguez, and A. C. Smith, "Supply induced interharmonic effects in wound rotor and dfigs," *IEEE Trans. Energy Convers.*, vol. 30, no. 4, pp. 1397–1408, 2015.

[12] G. Mv and N. P. Padhy, "PHIL experimentation on fault ride through behavior of doubly fed induction generator based wind system in the presence of fault current limiter," *IEEE Trans. Ind. Appl.*, pp. 1–1, 2020.

[13] N. Jabbour, E. Tsioumas, C. Mademlis, and E. Solomin, "A highly effective fault-ride-through strategy for a wind energy conversion system with DFIG," *IEEE Trans. Power Electron.*, pp. 1–1, 2020.

[14] H. Nian and Y. Jiao, "Improved virtual synchronous generator control of DFIG to ride-through symmetrical voltage fault," *IEEE Trans. Energy Convers.*, pp. 1–1, 2019.

[15] Y. Deng, Z. Xing, and Q. Zhang, "Analysis of electromagnetic transient characteristics of DFIG under grid voltage swell," *CPSS Trans. Power Electron. Appl.*, vol. 3, no. 2, pp. 111–118, Jun. 2018.

[16] M. Vicatos and J. Tegopoulos, "Transient state analysis of a doubly-fed induction generator under three phase short circuit," *IEEE Trans. Energy Convers.*, vol. 6, DOI 10.1109/60.73790, no. 1, pp. 62–68, 1991.

[17] G. Pannell, D. J. Atkinson, and B. Zahawi, "Analytical study of grid-fault response of wind turbine doubly fed induction generator," *IEEE Trans. Energy Convers.*, vol. 25, no. 4, pp. 1081–1091, Dec. 2010.

[18] S. Tohidi, "Analysis and simplified modelling of brushless DFIM in synchronous mode of operation," *IET Elect. Power Appl.*, vol. 10, no. 2, pp. 110–116, 2016.

[19] M. Yousefian, H. A. Zarchi, and H. Gorginpour, "Modified steady-state modelling of brushless DFIG taking core loss components into account," *IET Elect. Power Appl.*, vol. 13, DOI 10.1049/iet-epa.2019.0133, no. 9, pp. 1402–1412, 2019.

[20] Z. M. Salameh and L. F. Kazda, "Analysis of the double output induction generator using direct three-phase model part ii - harmonic analysis," *IEEE Trans. Energy Convers.*, vol. EC-2, no. 2, pp. 182–188, 1987.

[22] D. Kim, Y. Moon, and H. Nam, "A new simplified doubly fed induction generator model for transient stability studies," *IEEE Trans. Energy Convers.*, vol. 30, no. 3, pp. 1030–1042, Sep. 2015.

[21] M. Zhou, Z. Dong, H. Li, C. Gan, G. Li, and Y. Liu, "Coordinated control of dfig based wind farms and sgs for improving transient stability," *IEEE Access*, vol. 6, pp. 46 844–46 855, 2018.

[23] F. Maurer and J. K. Nøland, "An analytical model for detailed transient fault analysis of doubly-fed induction machines," in *Proc. Int. Conf. Electr. Mach. (ICEM)*, vol. 1, pp. 1287–1293, 2020.

[24] K. W. Kanelis, "Analytical equations of the induction machine," in *Proc. Int. Conf. Elect. Mach. (ICEM)*, pp. 2854–2860, Sep. 2016.

[25] J. Chatelain, "Machines electriques, volume x," *Traite d'electricite series, Presses Polytechniques. PPUR, Lausanne, ppur Edition*, 2013.

[26] I. Canay, "Extended synchronous-machine model for the calculation of transient processes and stability," *Electric machines and Electromechanics*, vol. 1, no. 2, pp. 137–150, 1977.

[27] F. M. Maurer, "Electrical effects in winding of large electrical AC machines application to advanced large size DFIM," EPFL, Tech. Rep., 2019.

[28] F. Maurer, M. T. Xuan, and J. Simond, "Two full parameter identification methods for synchronous machine applying DC-decay tests for a rotor in arbitrary position," *IEEE Trans. Ind. Appl.*, vol. 53, no. 4, pp. 3505–3518, Jul. 2017.

[29] F. Maurer, "Determination des parametres de la machine synchrone par essais "DC-Decay"," *Master thesis, EPFL*, 2009.

[30] A. Hodder, "Double-fed asynchronous motor-generator equipped with a 3-level vsi cascade," EPFL, Tech. Rep., 2004.

[31] H. Buhler, *Reglage de systéme d'électronique de puissance (Volume 3)*. EPFL Lausanne: PPUR, 1999.

Frederic Maurer received his M.Sc. degree in 2009 and the Ph.D. degree in 2019 from the Swiss Federal Institute of Technology in Lausanne (EPFL). Since April 2009, he is working for Alstom Hydro (now GE Hydro) in differents positions: R&D engineer in the generator technology center, Lead electrical engineer, and technical project manager. From February 2021, he is a guest researcher at the Department of Electric Power Engineering, Norwegian University of Science and Technology. His current research interests include circulating current, electromagnetics, improved utilization of electrical machines, and electricity market design. Dr. Maurer regularly serves as a Reviewer for IEEE journals and conferences.

Trond Leiv Toftevaag (M'99) was born in Bergen, Norway, 1949. He received the "Sivilingeniør" degree from the Norwegian University of Science and Technology, NTNU (previously NTH), Department of Electric Power Engineering, Trondheim, in 1972. After several years in the shipping industry and consultancy, he was employed as a research scientist at SINTEF Energy Research (former EFI) in Trondheim in 1979. Since 2013 he has been a full-time associate professor, in 2018 promoted to docent/professor at the Department of Electric Power Engineering (IEL), NTNU. His technical interests are electrical machines, power system dynamics, and modeling and simulation of electrical power systems.

Jonas Kristiansen Nøland (S'14-M'17) was born in Drammen, Norway, in 1988. He received the M.Sc. degree in electric power engineering from the Chalmers University of Technology, Gothenburg, Sweden, in 2013, and the Ph.D. degree in engineering physics from Uppsala University, Uppsala, Sweden, in 2017. Since 2018, he has been an Associate Professor with the Department of Electric Power Engineering, Norwegian University of Science and Technology. His current research interests include excitation systems, hydrogenerators, large AC machines, and enhancing their utilization. Dr. Nøland serves as an Editor for the IEEE TRANSACTIONS ON ENERGY CONVERSION and as an Associate Editor for the IEEE TRANSACTIONS ON INDUSTRIAL ELECTRONICS.